Article

Scaling of internal organs during *Drosophila* embryonic development

Prabhat Tiwari,[1] Hamsawardhini Rengarajan,[1] and Timothy E. Saunders[1,2,3,4,*]

[1]Mechanobiology Institute and [2]Department of Biological Sciences, National University of Singapore, Singapore, Singapore; [3]Institute of Molecular and Cell Biology, A*Star, Singapore, Singapore; and [4]Warwick Medical School, University of Warwick, Coventry, United Kingdom

ABSTRACT   Many species show a diverse range of sizes; for example, domestic dogs have large variation in body mass. Yet, the internal structure of the organism remains similar, i.e., the system scales to organism size. *Drosophila melanogaster* has been a powerful model system for exploring scaling mechanisms. In the early embryo, gene expression boundaries scale very precisely to embryo length. Later in development, the adult wings grow with remarkable symmetry and scale well with animal size. Yet, our knowledge of whether internal organs initially scale to embryo size remains largely unknown. Here, we utilize artificially small *Drosophila* embryos to explore how three critical internal organs—the heart, hindgut, and ventral nerve cord (VNC)—adapt to changes in embryo morphology. We find that the heart scales precisely with embryo length. Intriguingly, reduction in cardiac cell length, rather than number, appears to be important in controlling heart length. The hindgut, which is the first chiral organ to form, displays scaling with embryo size under large-scale changes in the artificially smaller embryos but shows few hallmarks of scaling within wild-type size variation. Finally, the VNC only displays weak scaling behavior; even large changes in embryo geometry result in only small shifts in VNC length. This suggests that the VNC may have an intrinsic minimal length that is largely independent of embryo length. Overall, our work shows that internal organs can adapt to embryo size changes in *Drosophila*, but the extent to which they scale varies significantly between organs.

SIGNIFICANCE   How do organs adjust position and size (i.e., scale) to changes in organism size? This question has received significant research focus over the past 100 years, but it is still poorly understood how (if they even do) internal organs scale during embryo development. Here, using quantitative approaches and genetically induced smaller embryos, we show that three organs within the developing *Drosophila* embryo display distinct scaling properties. The heart adjusts its size to scale with embryo length by altering the cardioblast morphology. However, the ventral nerve cord appears to have a minimal absolute size. Our results show that organ scaling can occur early in development, but the effects of such scaling can be highly organ specific.

INTRODUCTION

Organism scaling (allometry), including in humans, is an important developmental process (1). A striking example is the large variation because of selective breeding in domestic dog size, from ∼2–3 kg to ∼70 kg; yet they are genetically very similar (2). The extent to which an organ grows is regulated by the body size of the individual. Understanding the processes that drive organism scaling has been a longstanding challenge in developmental biology (3,4). In recent years, the study of external organs such as the insect wing (5–7) and beetle horns (8) has provided novel insights

into the relationship between organ and organism size and the associated physiological properties (9).

What are the mechanisms controlling organ size? In the case of winged organisms, they require extremely precise regulation of the wing size, including left-right symmetry, to ensure optimal flying (10). Such regulation could be driven by both genetic and mechanical processes within the organ (11,12). In *Manduca sexta*, wing size is tightly regulated by the adult body size. This regulation is achieved through altering the cell number in the wing disk (5). Mechanical processes can act through direct limitation on tissue growth or by inducing mechanosensitive pathways (13–17). The timing of signal interpretation and external hormonal inputs can also direct organ scaling (6,18–20), and neighboring organs can regulate organogenesis (21). Theoretical approaches have also been important in

deciphering the possible processes driving precise scaling (22).

Arguably, the best quantified system for studying scaling in development is gene expression boundary specification along the anterior-posterior (AP) axis in the early *Drosophila* embryo (23). Such boundaries scale precisely with embryo length (E_L), with an error of less than one cell diameter. These boundaries are downstream of the morphogen gradient Bicoid and other maternal inputs (24,25). The scaling of the boundaries is robust to natural variations in both Bicoid levels and embryo size, but the scaling does break down under larger changes in either Bicoid or embryo size (26,27).

Later in *Drosophila* development, there has been extensive research into how larval organs grow and adapt to environmental stresses (28–30). These organs form first in the embryo and are derived from the precisely scaled patterns laid down in the early embryo (31). During the larval and pupal stages, most of these organs undergo substantial reconfiguration (30), including large-scale removal of the initial embryonic cells. So, whether these initial embryonic organs need to scale and adjust to changes in embryo size is an open question. Dissecting organ scaling is complicated by the diverse range of organ formation processes and morphologies. For example, in *Drosophila*, muscle growth occurs through myoblast fusion and elongation (32), the hindgut grows by chiral reorientation of cells (33), the ventral nerve cord (VNC) undergoes large-scale elongation followed by condensation (34,35), and the heart forms from a fixed number of cells (31,36).

Here, taking advantage of the imaging accessibility of the *Drosophila* embryo and a mutant that produces smaller (yet still viable) embryos, we provide quantitative measures of the formation and scaling of three internal organs: the heart, hindgut, and VNC. These three organs have distinct characteristics that make them particularly pertinent for exploring scaling. The *Drosophila* heart is a linear tube oriented along the embryo AP axis with fixed cell number (31,36). The regulatory gene network determining heart specification is highly conserved between species—along with the initial heart morphology—and so insights into scaling of the early heart may have relevance in higher organisms (37). The hindgut is the first chiral organ to emerge during *Drosophila* development, taking on a distinct curved morphology (38,39). Typically, scaling studies have focused on tissues with simple morphologies whose shape can effectively be described by a single parameter (10). The hindgut offers an opportunity to test whether chiral tissues scale and, if so, whether they scale equally along different axes. The VNC is a unique organ that spans across the entire embryo length before condensing by means of apoptosis and long-range coordinated mechanical interactions (40,41). As the VNC shrinks, rather than grows, to its final size within the embryo, its mechanisms of size control are likely distinct from well-studied systems such as the *Drosophila* wing

disk (12). Intriguingly, here we show that these three organs each display distinct scaling characteristics, suggesting that embryonic internal organs are highly variable in how they respond to changes in organism size.

MATERIALS AND METHODS

Generation of artificially smaller embryos

In wild-type (control) embryos, the natural variation is ∼10% in embryo length (Fig. 1, *A* and *B*) and 13% in embryo width (Fig. 1, *A* and *C*). This small variability makes studying scaling within the embryo challenging. To get around this problem, we utilized *TrafficJam-Gal4>UAS-fat2-RNAi* (henceforth referred to as *TjGal4>fat2RNAi*)-expressing flies (27,42), which lay shorter embryos along the AP axis, although they have larger width (Fig. 1, *A–C*). Embryos labeled as *TjGal4>fat2RNAi* are laid by females of the genotype *TjGal4>fat2RNAi*. Importantly, these eggs are viable and typically result in healthy larvae (Video S1). This manipulation provided 30% variation in the E_L and 20% variation in the embryo width (E_W). The control embryos have a length distribution of 473–572 μm and width distribution of 150–195 μm. In *TjGal4>fat2RNAi* animals, the eggs laid on the first day after setting up the cage typically consisted of eggs close in size to wild-type. Here, we have taken *TjGal4>fat2RNAi* embryos ranging from 362 to 465 μm. In Fig. 5, in which we used *TjGal4>fat2RNAi* embryos of 470 and 490 μm length (laid soon after cage setup) to serve as an internal control, embryo length is correlated with embryo width in the *TjGal4>fat2RNAi* embryos, but not in control (Fig. 1 *D*). Comparing the embryo length with the aspect ratio (length/width), we see a clear correlation in controls and *TjGal4>fat2RNAi* embryos (Fig. 1 *E*). As reported previously (27), this corresponds to the *TjGal4>fat2RNAi* embryos only having a small decrease in total volume compared with wild-type embryos.

Fly stocks

We used the following fly lines in this work: *Tj*Gal4 (43), UAS-*fat2*RNAi (VDRC27114 and BDSC40888), Hand::GFP and *Hand*-Gal4 (44), UAS-moe::GFP (45), *elav*Gal4>UAS-GFP (BDSC5146), *Byn*Gal4>UAS-myr::GFP (46), *Byn*::mtdTomato (from Kenji Matsuno), *Histone*::RFP (BDSC 23650), *Myo31DF^{L152}*, and *Byn*Gal4>UAS-myr::GFP (46). In the heart experiments, our control line was Hand::GFP. In the VNC experiments, our control line was *elav*Gal4>UAS-GFP. In the hindgut experiments, our control line was *Byn*::mtdTomato. We confirmed that *Byn*>Gal4-UAS>myr::GFP UAS-*fat2*-RNAi showed similar behavior to our control embryos for the hindgut.

Imaging protocols and microscope

We used NikonA1R (Tokyo, Japan) and Zeiss LSM 700 (Oberkochen, Germany) confocal microscopes for time-lapse imaging. We picked the desired stage embryos from the apple agar plate and dechorionated them using bleach. Embryos were then washed in phosphate-buffered saline and mounted on the coverslip dish in the desired orientation (dorsally for heart and hindgut and laterally for VNC). Time-lapse imaging was performed on a confocal microscope with time interval of 5–10 min. Recordings were taken at room temperature, typically 21–23°C. All data are collected from live videos except Video S5, which is immunostained for GFP and DE-Cad following standard immunostaining protocols. Chick anti-GFP (1:10,000; Abcam, Cambridge, UK) and rat-DCAD2 (1:300; Developmental Studies Hybridoma Bank, University of Iowa, Iowa City, IA) primary antibodies were used to label the GFP-expressing cells and DE-Cad expression, respectively. The primary antibodies were detected with AlexaFluor-labeled secondary antibodies (1:400; Invitrogen, Carlsbad, CA).
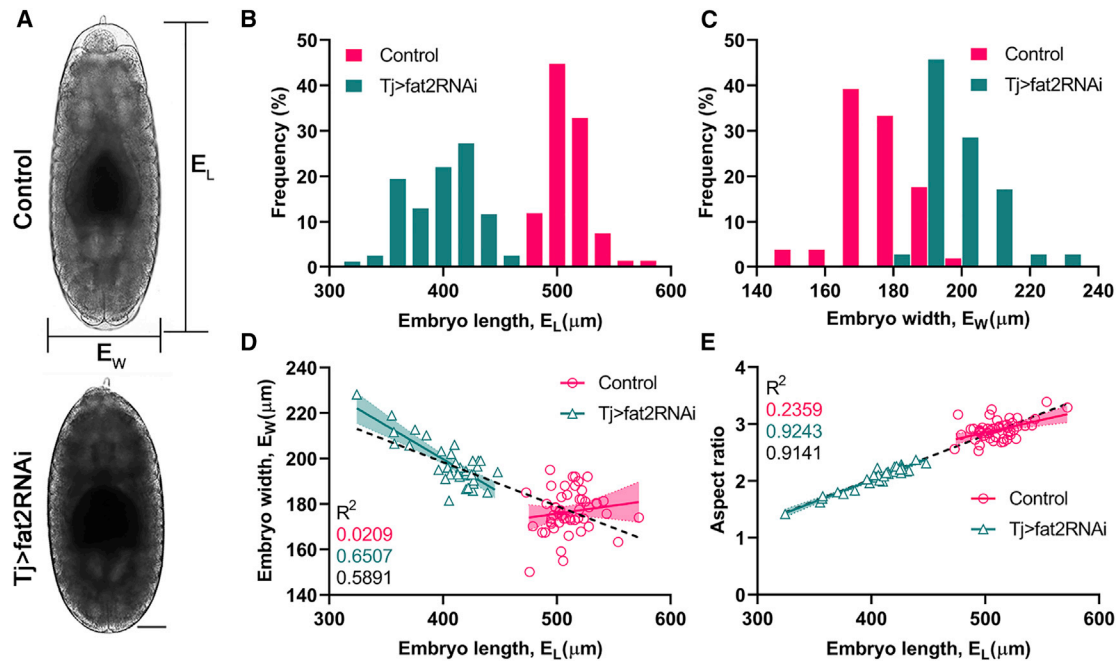
FIGURE 1 Quantification of embryo morphology in control and TjGal4>fat2RNAi embryos. (*A*) Brightfield images of stage 14 wild-type (control) and *TjGal4>fat2RNAi* embryos on same scale. (*B*) Distribution of embryo length in control and *TjGal4>fat2RNAi* embryos. (*C*) Distribution of embryo width in control and *TjGal4>fat2RNAi* embryos. (*D*) Correlation of embryo length with embryo width in control and *TjGal4>fat2RNAi* embryos. (*E*) Correlation of aspect ratio with embryo length. For (*B*), n = 67 (control) and n = 77 (*TjGal4>fat2RNAi*); for (*C*)–(*E*), n = 51 (control) and n = 35 (*TjGal4>fat2RNAi*). Scale bars in (*A*), 50 μm. Shaded regions represent 95% confidence interval on the linear fitting and r²-values given in the legend, color coded by control (*magenta*), *TjGal4>fat2RNAi* (*cyan*), and all data (*black*). To see this figure in color, go online.

Image analysis details

Embryo length and width were measured in ImageJ (National Institutes of Health, Bethesda, MD) manually as shown in Fig. 1 *A*.

Heart quantification

At stage 14, we measured the two rows of cardioblasts once they clearly move inward from a dorsal view. For each embryo, we measured both rows of cardioblasts and averaged the values for each embryo (Fig. 2, *A*–*C*). For each embryo, we measured the distance between the anteriormost and posteriormost ends of both rows and averaged these values. We used this value to measure the heart arching at stage 14. At stage 16, we measured the size of the heart immediately after both rows of cardioblasts met at the dorsal midline.

VNC quantification

VNC length measurements were done by drawing a segmented line along the VNC in ImageJ at two developmental time points (Fig. 4, *A* and *B*): the onset of stage 15 (we used the gut morphology to identify this specific landmark) and during stage 17, just before clear tracheal filling.

Hindgut quantification

Hindgut measurements (Fig. 6, *A* and *B*) were done at the developmental time point when the hindgut reached its maximal distance along AP axis before twisting (during stage 14). Distances along the AP axis were measured from the anus in the posterior manually on ImageJ. Curvature was measured by fitting a circle to the region highlighted in Fig. 6 *B*. Because the hindgut anterior end is not perfectly circular in its morphology, we fitted the circle to the highlighted dark blue region in Fig. 6 *B*. For each data set, all embryos within the cohort were quantified before any statistical analysis to reduce potential for bias. Only embryos that displayed clear evidence of sickness were excluded from the analysis.

Statistical analysis

All statistical analysis was performed in GraphPad (GraphPad Software, San Diego, CA) except for the bootstrapping analysis (Fig. 4 *E*). For calculating the *p*-value between measured means, we used Welch's test (unpaired *t*-test with Welch's correction). To test whether observed scaling relationships showed statistically significant differences from no correlation (null hypothesis was that there would be a zero gradient in the linear fit), we used GraphPad's built-in regression-slope test. We further provide r²-values on all linear fittings in the figure panels. In all linear regression analyses, we show the 95% confidence interval (*shaded regions* in figure panels). In Fig. 4 *E*, error on the VNC embryo-to-embryo variability was calculated through bootstrapping using the MATLAB (The MathWorks, Natick, MA) function *bootstrp*. 100 random samples were generated for each condition.

RESULTS

The *Drosophila* heart scales with embryo length

The *Drosophila* heart is a tubular structure with no change in cell number during its formation (48). The two rows of cells (52 cells each) migrate from the two lateral sides of embryo (at developmental stage 14) toward the dorsal midline (Video S2). They match precisely at the dorsal midline in developmental stage 16 to form the dorsal vessel (49,50). In stage 14, the two rows of cells arrange in arched structures (Fig. 2 *A*). In stage 16, the heart has a simple linear structure (Fig. 2 *B*). From imaging embryos expressing heart-specific markers (Materials and methods), we can

quantify the heart shape during morphogenesis in differently sized embryos (Fig. 2 *C*).

At stage 14, we see that the future heart in *TjGal4>fat2RNAi* embryos is shorter in total length ($H_{L14} = 209 \pm 9$ μm) than control embryos ($H_{L14} = 235 \pm 14$ μm) (Fig. 2, *D* and *E*). Further, the heart is more arched in *TjGal4>fat2RNAi* embryos compared with stage 14 control embryos (Fig. 2 *D(ii)*). At stage 14 in control embryos, the length of the future heart sections scales with the embryo length ($p < 10^{-3}$), but not with the embryo width ($p = 0.33$) (Fig. 2, *D* and *E*). In the *TjGal4>fat2RNAi* embryos at stage 14, there is not significant scaling of heart length with the embryo size ($p = 0.11$ and 0.32 for embryo length and width, respectively). We define the heart arching as H_{I14}/H_{L14}; a straight heart would have an arch of 1, with the value of H_{I14}/H_{L14} decreasing for more curved hearts. There is a weak scaling between the heart arch extent in stage 14 and embryo length within each data set ($p = 0.04$ for control embryos, Fig. 2 *E(ii)*), but when combining the data sets, we see a clear trend for increasingly arched hearts at stage 14 in shorter, wider embryos (Fig. 2 *E(ii)*).

At stage 16, control and *TjGal4>fat2RNAi* embryos show clear scaling with embryo length ($p < 10^{-3}$ for both conditions, Fig. 2 *F*). The correlation between embryo and heart length is substantially increased compared with stage 14 embryos. This suggests that the heart length adjusts to embryo size during its formation. This strong scaling is remarkable for two reasons: 1) the heart is constructed of a fixed cell number, and 2) the scaling becomes more apparent later in embryonic development. Given the linear nature of the heart orientated along the AP axis, unsurprisingly, we do not see scaling of heart size with embryo width (Fig. 2 *G*).

The embryonic *Drosophila* heart scales by reducing cell length along the AP axis

Given the clear scaling of the stage 16 heart with embryo length, we asked what morphological changes occur to ensure such scaling? Two possibilities are that the cardioblasts change morphology or that the number of heart cells is reduced. To count the number of cardioblasts, we used Hand::GFP, which marks the nuclei of the cardioblasts and surrounding pericardial cells, which are readily distinguished by position (Fig. 3 *A*). We counted the number of heart cells in control and *TjGal4>fat2RNAi* embryos. We found that the number of cardioblasts on each side of the embryo remained constant, with 52 per embryo, even in very short embryos (Fig. 3 *B*), showing that heart scaling is independent of cell number.

To test whether the cell size along the AP axis was altered, we imaged cardioblast morphology using *Hand*-Gal4>UAS-Moe::GFP, which marked the cell boundaries (Fig. 3 *C*). We observed a clear decrease in the cell length along the AP axis, with 5.0 ± 0.7 μm (control) and 3.6 ± 0.7 μm (*TjGal4>fat2RNAi*), $p < 10^{-3}$ (Fig. 3, *C* and *D*).

The heart is composed of a repeating pattern of four Tinman-positive and two Seven-up (Svp)-positive cardioblasts (47). The Svp-positive cardioblasts form ostia and are generally narrower than the Tinman-positive cells. In Fig. 3 *C*, we highlight the Svp-positive cardioblasts (*red brackets*). Within the same spatial region, there are two sets of Svp-positive cardioblasts in the control embryo compared with three sets in the *TjGal4>fat2RNAi* embryos. Overall, we see that by stage 16, the heart scales with embryo length and this is mediated by a change in heart cell morphology, not cell number.

The VNC weakly adjusts to embryo size changes

The VNC, a part of the *Drosophila* central nervous system, is first specified ventrally during germband elongation (stage 8 onward). By stage 11, the developing VNC along with the germ band extends to the dorsal side. Then, from stage 12 onward it retracts along with the germband. By stage 17, it has reduced in size to 60% of the embryo length (31,35) and resides near the ventral surface (Fig. 4 *A*; Video S3). During the condensation process, a significant number of cells die through apoptosis (40,51). We measured VNC length at stage 15 and late stage 17 (Materials and methods) in control and *TjGal4>fat2RNAi* embryos and compared it to the embryo length. At stage 15, the total VNC length V_{L15} (Fig. 4 *B*) was 442 ± 13 and 403 ± 16 μm for control and *TjGal4>fat2RNAi* embryos, respectively (for control (n = 16) and *TjGal4>fat2RNAi* (n = 34), $p < 10^{-3}$, difference in means). The total VNC length in *TjGal4>fat2RNAi* embryos was around 10% shorter than in control ($p < 10^{-3}$, difference in means). In stage 17, the total VNC length in *TjGal4>fat2RNAi* embryos was also around 10% shorter than control conditions (267 ± 23 and 235 ± 14 μm for control (n = 16) and *TjGal4>fat2RNAi* (n = 23), $p < 10^{-3}$, difference in means).

The total VNC length correlated with embryo length at stage 15 in both control and *TjGal4>fat2RNAi* embryos (Fig. 4 *C(i)*). Interestingly, the linear length of the VNC along the AP axis (V_{AP15}) scaled more strongly with embryo length in the *TjGal4>fat2RNAi* embryos (Fig. 4 *C(ii)*). However, by stage 17 this correlation was largely lost in both control and *TjGal4>fat2RNAi* embryos (Fig. 4 *D*). In particular, despite the large changes in embryo geometry (embryo length between 347 and 465 μm) in *TjGal4>fat2RNAi* embryos, we saw no clear correlation between the VNC total length and the embryo length (Fig. 4 *D(i)*). As with stage 15, there is slightly stronger scaling with embryo length when we analyze the linear length of the VNC along the AP axis (Fig. 4 *D(ii)*). When we compare the mean total VNC length in control and *TjGal4>fat2RNAi* embryos in stage 17, we do see a small change in length, but this is less than 10% of the mean VNC length (compared with ~30% shortening in embryo length). These results suggest that during the final stages of VNC condensation
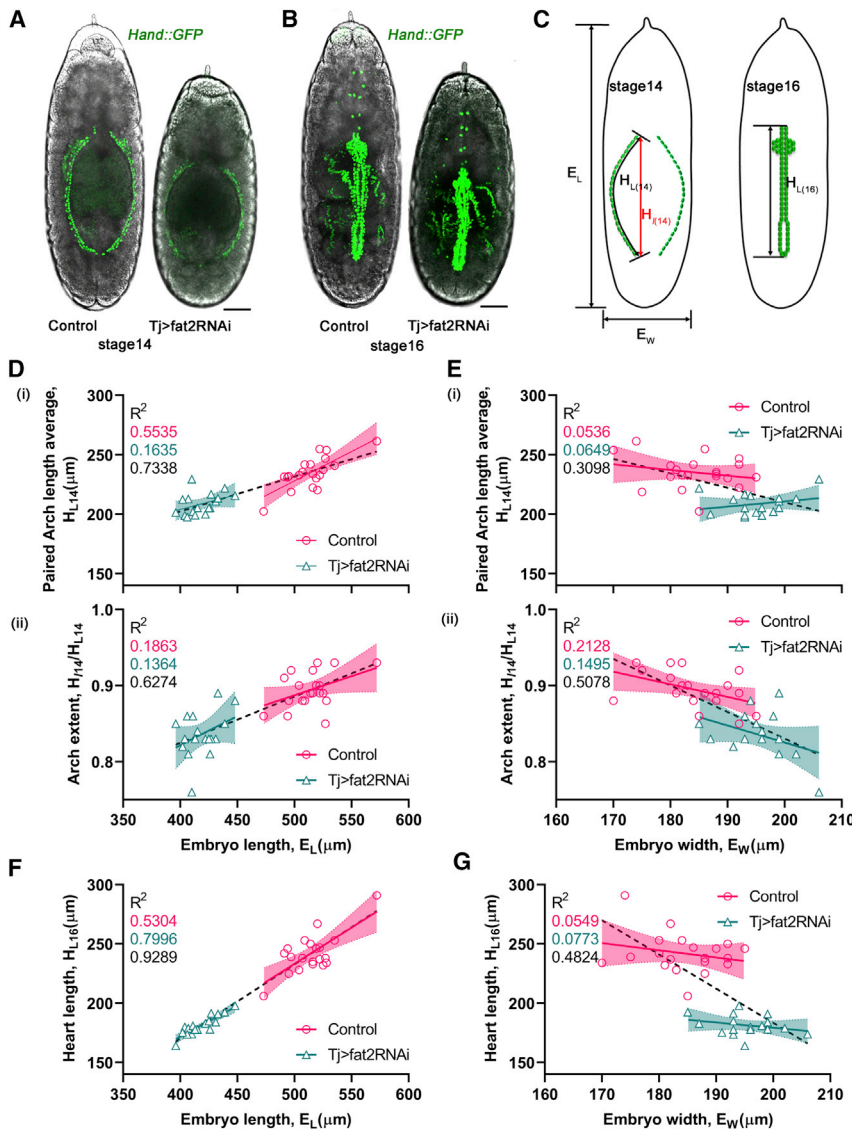
FIGURE 2 Scaling of the *Drosophila* embryonic heart. (*A*) Two contralateral opposite rows of heart cells at stage 14 in control and *TjGal4>fat2RNAi* embryos marked by Hand::GFP (Materials and methods). (*B*) Stage 16 heart cells align close to each other to form the heart tube (47). (*C*) Schematic showing different measurements used in analysis: $H_{L(14)}$ and $H_{L(16)}$ are the total length of heart at stages 14 and 16, respectively, and H_{I14} is the linear distance between the anterior and posterior end of the row of cells at stage 14. (*D*) Correlation with embryo length at stage 14 of average total heart length, $H_{L(14)}$ (*i*), and arch extent, $H_{I(14)}/H_{L(14)}$ (*ii*). (*E*) Correlation with embryo width at stage 14 of average heart length at stage 14 (*i*), and arch extent (*ii*). (*F* and *G*) Correlation of heart length at stage 16, $H_{L(16)}$, with embryo length (*F*) and width (*G*) for control embryos (n = 20) and for *TjGal4>fat2RNAi* embryos (n = 17). Shaded regions represent 95% confidence interval on the linear fitting and r^2-values given in the legend, color coded by control (*magenta*), *TjGal4>fat2RNAi* (*cyan*), and all data (*black*). All scale bars represent 50 μm. To see this figure in color, go online.

(stages 16 and 17), the VNC length only weakly adapts to the surrounding embryonic environment.

This behavior motivated us to explore the variability in VNC length during development. Looking at the variation in VNC length in control conditions (n = 16 embryos), we saw that the VNC length is highly robust between embryos, even though the embryos have variable length (478–536 μm) (Fig. 4 *E*). The relative error in the VNC length was less than 4% in control embryos. The variability was larger in *TjGal4>fat2RNAi* embryos but still less than 10% variation. We also found the absolute error in the total VNC length (normalized by average VNC length). The VNC length variation between embryos was 3 and 4% for control and *TjGal4>fat2RNAi* embryos, respectively, in stage 15 and 9 and 6% for control and *TjGal4>fat2RNAi* embryos, respectively, in stage 17. The embryo-to-embryo variability in VNC length was

less than 10% of its typical length in both control and *TjGal4>fat2RNAi* embryos, regardless of embryo length. This is remarkably small variation for an organ that undergoes such large-scale morphological changes. These results suggest that the final total VNC length may have a preferred intrinsic length and perhaps even a minimal size requirement (>220 μm in stage 17), although further work is required to test these ideas. A prediction stemming from these observations is that in very short embryos, the VNC may deform, as there could be insufficient space for it to occupy the ventral surface. In one *TjGal4>fat2RNAi* embryo (which displayed muscle twitching but did not hatch), we indeed observed buckling (Fig. 4 *F*). However, this buckling was not just in the VNC, so it is not possible to conclude clearly whether the VNC induced buckling or whether it was deforming because of other size pressures.
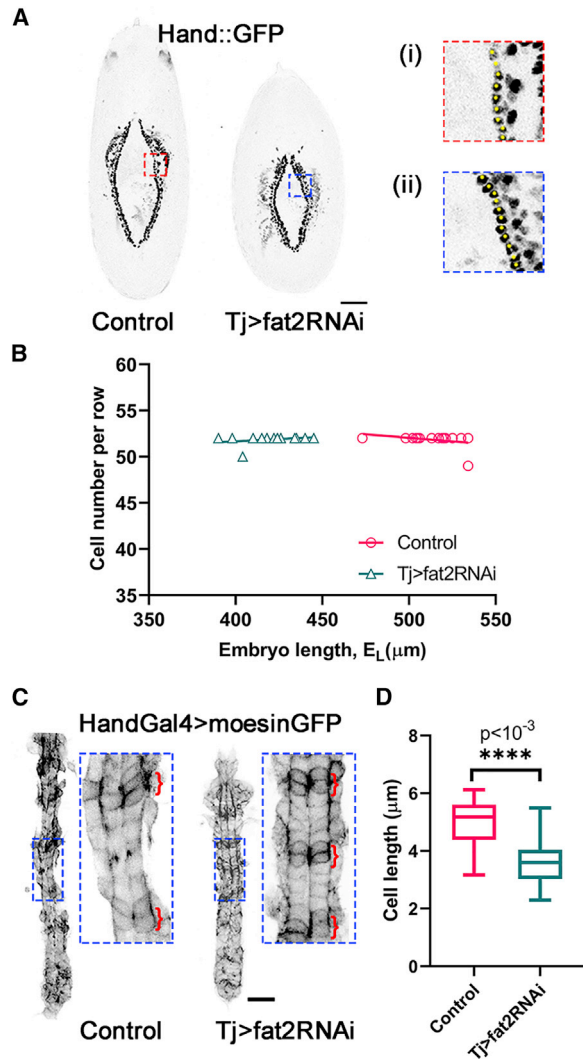
A

B

C

D

FIGURE 3 Scaling of the embryonic heart occurs through cell shape changes. (*A*) Heart cells (cardioblasts) with their nuclei labeled with Hand::GFP. (*i*) and (*ii*) correspond to zoomed in regions denoted by the red and blue boxes on left, respectively; cardioblasts are marked with yellow dots. (*B*) Cardioblast number against embryo length for control and *TjGal4>fat2RNAi* embryos, n = 17 (control), n = 15 (*TjGal4>fat2RNAi*). (*C*) *Hand*-Gal4>moe::GFP marking the cell boundary in the developing heart for control (*left*) and *TjGal4>fat2RNAi* (*right*) embryos. Red brackets highlight Svp-positive cells, which are narrower in the AP axis than Tinman-positive cardioblasts. The boxed regions are the same absolute size. (*D*) Mean cardioblast length in AP axis in control and *TjGal4>fat2RNAi* embryos (****$p < 10^{-3}$). Box represents 25–75% percentiles, and error bars are standard deviation. Lines in (*B*) represent a linear fitting with r^2-values given in the legend, color coded by control (*magenta*) and *TjGal4>fat2RNAi* (*cyan*). Scale bars in (*A*), 50 μm, and scale bars in (*C*), 20 μm. To see this figure in color, go online.

Although the overall size of the VNC did not change substantially in shorter embryos, we next asked whether there were changes in the local structure of the VNC. We looked at the ladder-like structure of the VNC and the emanating fascicles from the midline at the completion of head involution (Fig. 5 *A*). The fascicles originate at regular intervals

regardless of embryo size, with no apparent difference in their morphology (Fig. 5 *A*). Intercommissure distance (the distance between the ladder-like structures of the VNC) does appear to slightly decrease in shorter embryos (Fig. 5 *B*), consistent with Fig. 4, but there are no stark changes in small embryos. Therefore, the internal structure of the VNC appears to be morphologically similar in embryos of different lengths.

Scaling in the *Drosophila* hindgut, an asymmetric organ

The *Drosophila* hindgut is an asymmetric organ that grows largely by cell shape change (52) and not proliferation after stage 10 (53). To explore scaling of the *Drosophila* hindgut, we chose to examine the shape of the gut in stage 14. At this point, the hindgut forms a characteristic inverse "question-mark" shape (Fig. 6 *A*; Video S4). Given the chiral nature of the hindgut, we measured the organ curvature as well as its length and width in both control and *TjGal4>fat2RNAi* embryos (Fig. 6 *B*).

Measuring the total hindgut length (Hg_L) and its linear extent along the AP axis (Hg_H), we saw a clear decrease in the mean value for both Hg_L and Hg_H between wild-type (Hg_L 249 $\pm$ 7 μm and Hg_H 210 $\pm$ 6 μm) and *TjGal4>fat2RNAi* (Hg_L 209 $\pm$ 11 μm and Hg_H 166 $\pm$ 13 μm) embryos ($p < 10^{-3}$ for difference in means for both Hg_L and Hg_H). Looking at the correlation of Hg_L and Hg_H with embryo length (Fig. 6 *C*(*i* and *ii*)), we saw only very weak scaling in the control embryos ($p = 0.02$ for Hg_L and 0.12 for Hg_H), but stronger scaling in the *TjGal4>fat2RNAi* embryos ($p = 0.03$ for Hg_L and 0.001 for Hg_H). We also looked at how the hindgut width and curvature altered with embryo length. We observed distinct differences in hindgut width and curvature between control (width = 70 $\pm$ 3 μm and curvature = 0.034 $\pm$ 0.002 μm^{-1}) and *TjGal4>fat2RNAi* (width = 78 $\pm$ 7 μm and curvature = 0.029 $\pm$ 0.002 μm^{-1}) embryos. The hindgut width inversely scaled with embryo length in the *TjGal4>fat2RNAi* embryos (Fig. 6 *C*(*iii*), $p = 0.70$ and 0.002 for control and *TjGal4>fat2RNAi* embryos, respectively). This is likely related to the *TjGal4>fat2RNAi* embryos displaying an inverse relationship between embryo length and width (Fig. 1). Although the curvature decreased in *TjGal4>fat2RNAi* embryos, it did not show a clear scaling with embryo length (Fig. 6 *C*(*iv*)).

We saw similar behavior when looking at the geometric properties of the hindgut in comparison with embryo width (Fig. 6 *D*). In control embryos, there was negligible adjustment of hindgut morphology to changes in embryo width. However, in the *TjGal4>fat2RNAi* embryos, we saw more clear evidence for scaling ($p < 10^{-3}$) of Hg_H and Hg_W. This is possibly a consequence of the larger-scale morphological differences in the size of the eggshell in these embryos; both length (reduced) and width (increased) change
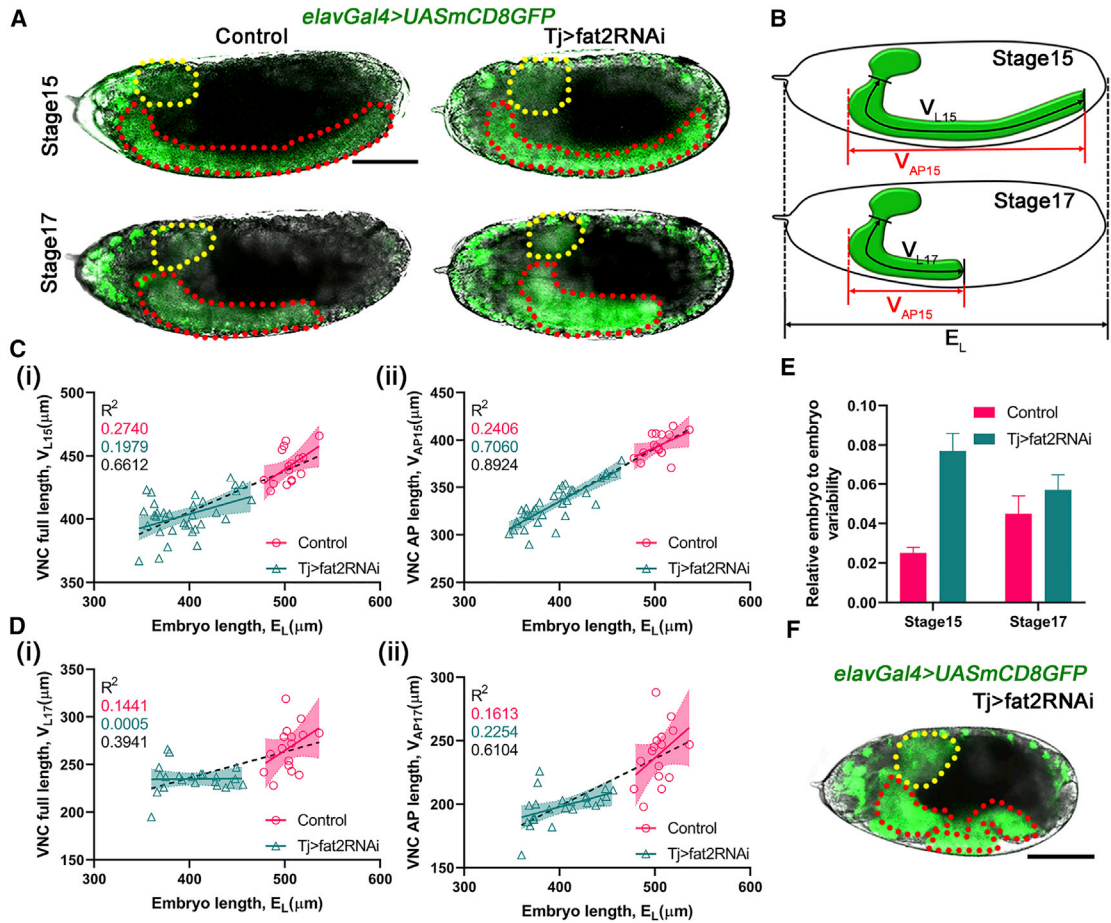
FIGURE 4 Scaling of the embryonic VNC. (*A*) Stage 15 and 17 control and *TjGal4>fat2RNAi* embryos (central nervous system (CNS) labeled in green by *elav*Gal4>UAS-GFP). Red and yellow dotted regions mark the VNC and brain, respectively. (*B*) Schematic showing the measurement method for the VNC length analysis; V_L is the length from the neck region of CNS to the posterior end of CNS, V_{AP} is the length of VNC along the AP axis, E_L is the embryo length on the AP axis, and numbers (15/17) in the subscript denote stage. (*C* and *D*) Correlation between total VNC length (*i*) and VNC length along AP axis (*ii*) with embryo length at stage 15 (*C*) and stage 17 (*D*). (*E*) Embryo-embryo variation in VNC length/embryo length at stages 15 (n = 16 and 34, respectively) and 17 (n = 16 and 23, respectively) for control and *TjGal4>fat2RNAi* embryos. Error bars found by bootstrapping (Materials and methods). (*F*) Example of buckling occurring in the VNC in a *TjGal4>fat2RNAi* embryo. All scale bars represent 100 μm. Shaded regions represent 95% confidence interval on the linear fitting and r^2-values given in the legend, color coded by control (*magenta*), *TjGal4>fat2RNAi* (*cyan*), and all data (*black*). To see this figure in color, go online.

considerably (Fig. 1), although total egg volume only decreased slightly. Overall, these results suggest that within wild-type variation in embryo size, the hindgut does not adjust significantly to embryo size variation. However, in the more stressed conditions provided by the *TjGal4>fat2RNAi* embryos, the hindgut can adjust to the changing physical environment. In particular, the increased width of *TjGal4>fat2RNAi* embryos appears to alter the shape of the hindgut; the width of the hindgut scales with embryo width in *TjGal4>fat2RNAi* embryos, but the curvature does not adjust linearly with embryo length or width.

To examine how the mechanical properties of the hindgut affect its ability to shape and whether this affects scaling, we analyzed $Myo1D^{-/-}$ embryos. Myo1D is a noncanonical myosin that plays a role in chirality formation, with such embryos often displaying an inverted hindgut (Fig. 7 *A*; (33)). Because of genetic limitations, we could not explore the effects of loss of Myo1D in *TjGal4>fat2RNAi* embryos. Instead, we focused on $Myo1D^{-/-}$ embryos which were wild-type-sized with 10-12% variation in embryo length and width respectively. The overall dimensions of the hindgut remain similar in $Myo1D^{-/-}$ embryos compared with control embryos despite the hindgut inversion. However, there was a much larger variation in hindgut morphology in $Myo1D^{-/-}$ embryos (as shown by the spread of 95% confidence intervals shown in Fig. 7, *B* and *C*). Note that we only analyzed $Myo1D^{-/-}$ embryos that showed a clear hindgut inversion. Furthermore, the curvature of the hindgut appears more sensitive to changes in embryo morphology (Fig. 7 *B(iv)*). $Myo1D^{-/-}$ embryos show slightly decreased curvature compared with control embryos (control = 0.034 ± 0.002, Myo1D = 0.032 ± 0.003, $p < 10^{-2}$, Fig. 7 *C(iv)*). As with our control embryos, the $Myo1D^{-/-}$ embryos showed no clear hallmarks of scaling with embryo length
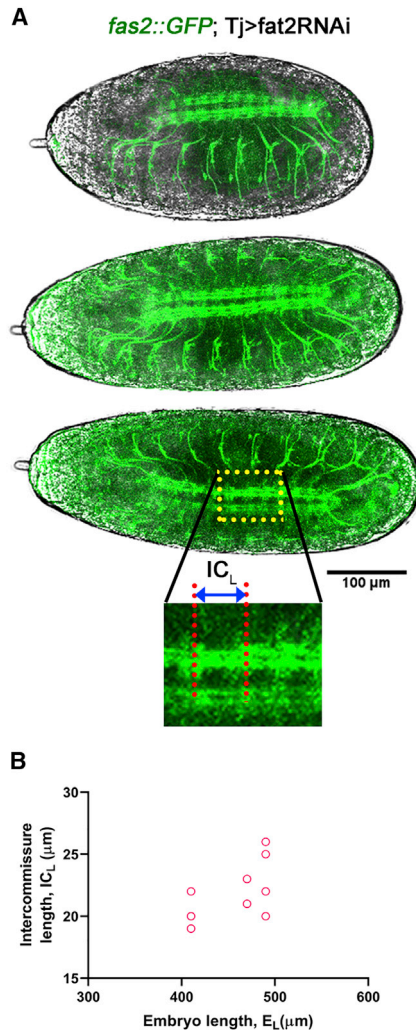
A *fas2::GFP*; Tj>fat2RNAi

B

FIGURE 5 Analysis of VNC structure in embryos of different length. (*A*) Differently sized *TjGal4>fat2RNAi* embryos expressing *Fas2GFP* showing the VNC and emanating fascicles. There is no apparent difference in the ladder-like structure among differently sized embryos. Inset in (*A*) shows the intercommisural distance labeled by the red dotted lines, denoted as IC_L. Scale bars, 100 μm. (*B*) Intercommissure length in the trunk region of the embryo for embryos of different lengths (for the shortest embryo, five measurements and four each for the two longer embryos; note that some data points are overlapping). To see this figure in color, go online.

or width. We conclude that disruption of Myo1D results in more than simply inverting the hindgut shape; there is much larger embryo-to-embryo variability between embryos, and the morphology of the hindgut is not simply an inversion of the "question-mark" geometry.

DISCUSSION

Most previous work that has quantified scaling at a cellular level has focused on external organs, such as the wing (10,12,54). Here, we have provided a dissection of scaling in three essential internal organs during *Drosophila* embryo development and shown that they display distinct scaling

characteristics. The heart scales strongly with embryo length in stage 16 (Fig. 2). The hindgut shows weaker scaling but does display some adaptation to changes in embryo size, particularly in *TjGal4>fat2RNAi* embryos (Fig. 6). Finally, the VNC length only weakly adjusts in size between embryos of significantly different morphology (Fig. 4). These results stand in stark contrast to the precision of gene networks early in the embryo (55,56), in which gene expression boundaries are closely scaled to embryo length. Our findings suggest that these gene boundaries are not translated into precisely scaled embryonic organs in general.

Our main observation is that the robustness of organ adjustment to changes in embryo size are quite distinct. Robustness in development is a longstanding problem given that many of the underlying processes are plastic in nature (57). For example, under starvation, growth of the ovaries is delayed in the *Drosophila* larvae (58), whereas the brain continues to develop similarly to healthy conditions for a substantially longer period (59–61). The VNC is constructed of a highly stereotypic repetition of specific neurons and connections (34,62). Larvae from *TjGal4>fat2RNAi* embryos quickly reach similar absolute size and morphology to larvae from control embryos. This is likely due to the total volume of the hatching larvae not being substantially different, as the volume of the egg in *TjGal4>fat2RNAi* embryos is only decreased slightly compared with control embryos (27). Therefore, the VNC may be sensitive to embryo volume, rather than specific size changes in one axis. This is plausible given the large size of the VNC before condensation. Overall, our results suggest that organs in the embryo adapt to specific changes in embryo size through organ-specific mechanisms.

Unlike most *Drosophila* organs, the embryonic heart is largely maintained throughout the fly life cycle (48). Therefore, there may be advantages to ensuring the heart is correctly sized from an early stage of development, as the organ is not substantially remodeled during either larval or pupal stages, limiting mechanisms that can adjust its size. We found that in heart scaling, the heart maintains cell number but changes cell size in smaller embryos. A range of organs regulate their size through modulating cell proliferation (5) or death (63,64). Instead, the heart cells appear to be mechanically malleable, enabling adjustment of size to fit within the constraining embryo environment. The mechanical structure of the heart cells has been analyzed by electron microscopy (65), although which mechanical processes are driving the dynamic morphological changes during heart formation remains unknown. The heart cells that form ostia (Svp-positive cardioblasts) are narrower than other heart cells. It has recently been shown that cell adhesion molecules Fas3 and Ten-m are precisely regulated between different heart cells, with disruption of Fas3 leading to changes in heart cell shape (49). It will be interesting in future work to explore whether the mechanical forces mediated by heterogenous expression of adhesion molecules play
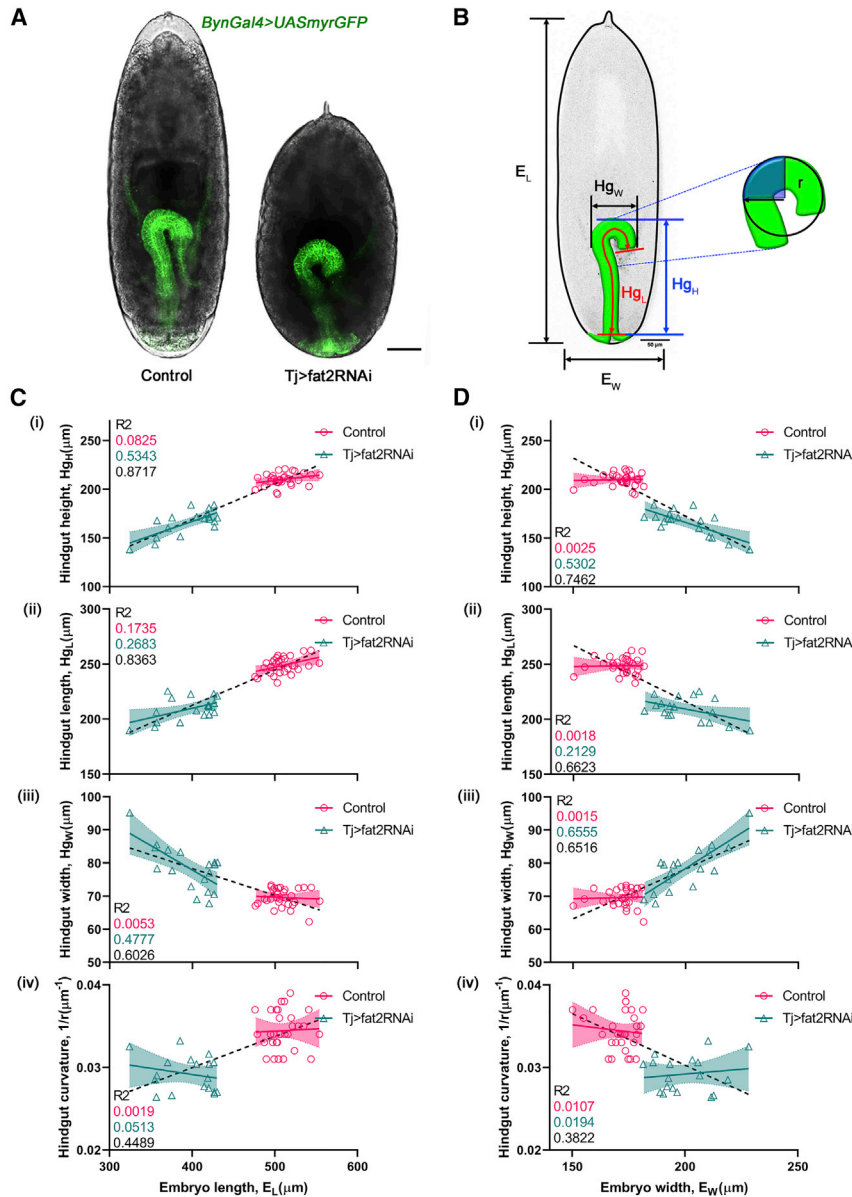
FIGURE 6 Hindgut scaling at stage 14. (*A*) Representative images of control (*left*) and *TjGal4>fat2RNAi* (*right*) embryos expressing *Byn*-Gal4>UAS-myr::GFP. Scale bars, 50 μm. (*B*) Schematic of measures used to quantify hindgut morphology. Inset shows how curvature was measured; we used the blue-shaded region to find the curvature, as the anterior end of the hindgut was not exactly circular. (*C* and *D*) Scaling of hindgut height Hg_H (*i*), total length Hg_L (*ii*), maximal width Hg_W (*iii*), and curvature (1/r) (*iv*) with embryo length (*C*) and width (*D*) in control (*magenta*) and *TjGal4>fat2RNAi* (*cyan*) conditions. Shaded regions represent 95% confidence interval on the linear fitting and r^2-values given in the legend, color coded by control (*magenta*), *TjGal4>fat2RNAi* (*cyan*), and all data (*black*) (n = 31 for control and n = 18 for *TjGal4>fat2RNAi*). To see this figure in color, go online.

an important role in determining the scaling properties of the heart.

The hindgut showed an intermediate response to changes in embryo size. In the hindgut, we see that the control embryos showed few characteristics of scaling, but in the (wider) *TjGal4>fat2RNAi* embryos, there is clear scaling behavior (Fig. 6, *C* and *D*). The surrounding organs may play an important role in restricting hindgut morphology. The midgut is positioned more anteriorly and may act to push against the hindgut as it extends. Further, the VNC lies beneath the hindgut, providing a barrier toward the ventral surface. Effectively, the surrounding organs may be acting to limit the available space for the hindgut, and such limitations may also explain the observed shape changes in hindgut morphology between control and *TjGal4>fat2RNAi* embryos. In particular, the wider *TjGal4>fat2RNAi* embryos may facilitate the hindgut to extend further in its width. In adult flies, the gut size varies between males and females (66). In future work, using our quantitative approach, we can explore whether these differences are apparent during embryogenesis. It will also be interesting to perturb the size of a specific organ and then explore how other organs adjust in size. Finally, we note that our analysis thus far has focused on the two-dimensional projected hindgut morphology in the AP lateral plane. However, the gut also extends in the dorsal-ventral (DV) axis (Fig. 7 *D*; Video S5). It is possible that the hindgut extends to differing degrees in the DV axis depending on constraints—for example, from neighboring organs. However, it is currently challenging to dissect the three-dimensional
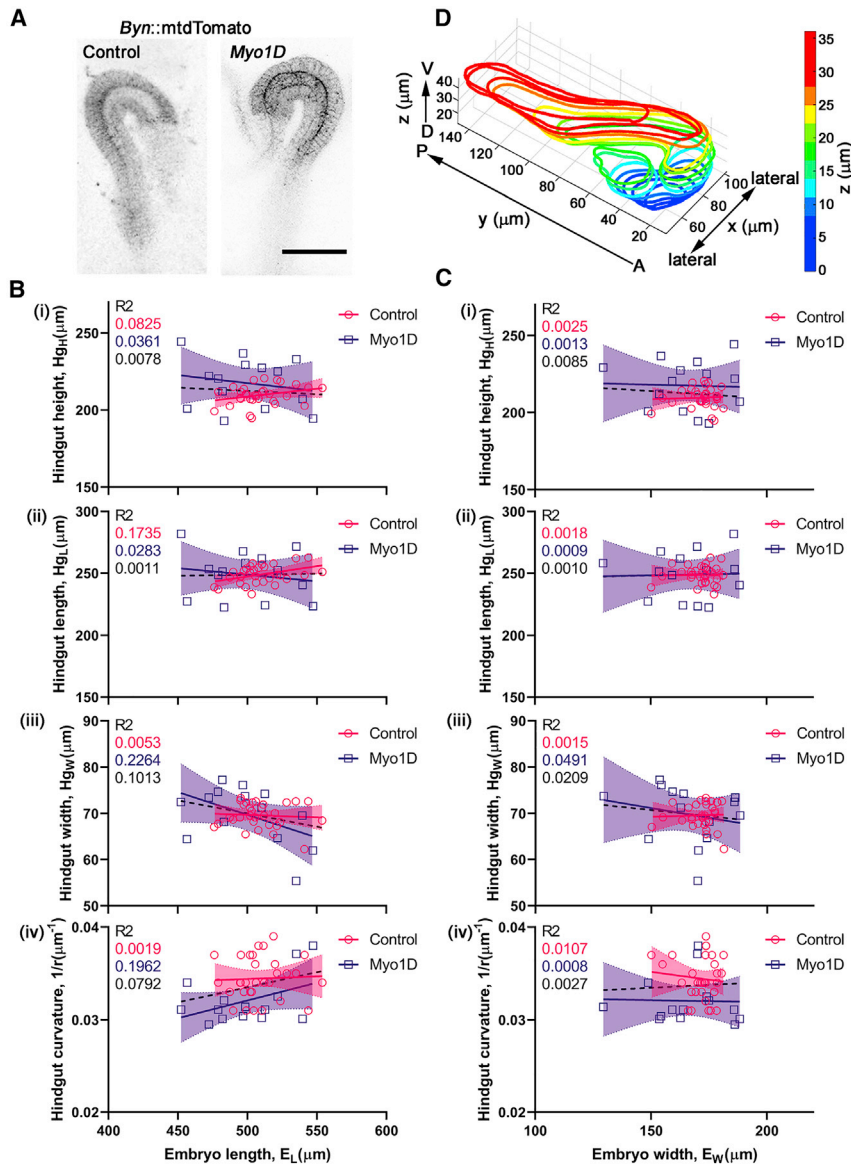
FIGURE 7 Hindgut scaling upon mechanical perturbation. (*A*) Representative images of the hindgut in control and *Myo1D*$^{-/-}$ embryos, expressing *Byn*-GFP>UAS-myr::GFP. Note the inverted hindgut compared with control. (*B* and *C*) Scaling of hindgut height Hg$_H$ (*i*), total length Hg$_L$ (*ii*), maximal width Hg$_W$ (*iii*) and curvature (1/r) (*iv*) with embryo length (*B*) and width (*C*) in control (*magenta*) and mutant (*purple*) conditions. (*D*) Three-dimensional segmentation of the hindgut in stage 14 (see also Video S5). Shaded regions represent 95% confidence interval on the linear fitting and r^2-values given in the legend, color coded by control (*magenta*), *Myo1D*$^{-/-}$ (*purple*), and all data (*black*) (n = 31 for control and n = 14 for *Myo1D*$^{-/-}$). Scale bars, 50 μm. To see this figure in color, go online.

gut morphology at cellular resolution in time-lapse videos, and so we do not consider this further here.

It is interesting to compare these results with other organisms. Dorsal-ventral scaling in the early *Xenopus* embryo is regulated by embryo-size-dependent degradation (67). By comparing different *Xenopus* species, evidence has also been found for transcriptional regulation of size (68). The formation of the skull depends on neural crest cell migration. By varying where and when neural crest cells migrate to specific regions of the developing skull, the resulting size of the skull can vary substantially between avian species (69). In mouse development, the formation of the proamniotic cavity depends on the size of the embryo (70). In humans, there have been extensive studies of size regulation of organ growth during childhood (71). The heart scales precisely with body mass during childhood (71). In contrast, the brain does not scale with body size, with rapid early growth followed by much slower change in mass. In humans, how the embryo regulates organ size during embryonic development remains largely unknown. There appears to be a large range of mechanisms to ensure precise scaling in different organisms. Our results further suggest that even within the developing embryo, the extent of organ scaling is potentially quite varied. Our study has focused on the embryonic stage of fly development, partly because of imaging accessibility for live, cellular-resolution imaging. Internal organ scaling may be differently regulated during larval and pupal stages, particularly given the large-scale remodeling processes that occur for the hindgut and VNC. Indeed, an interesting hypothesis is that the larval remodeling of organs may be able to correct for scaling errors from organ formation in the embryo.

Recent work has demonstrated that VNC condensation can be well described as a viscoelastic process, which generates oscillations in tissue length during condensation because of differences in the timescales over which the different mechanical interactions occur (41). Our work here shows that the VNC appears to only weakly scale with embryo length but does display evidence of a minimal viable size. Understanding how viscoelastic processes in active tissues regulate and respond to changes in tissue size remains an open problem in biophysics. Size regulation can depend on both mechanical and biochemical components working together (72). It will be interesting to explore whether gene expression profiles—which are tightly regulated within the heart and VNC in particular—show changes in response to external stresses, for example, in smaller embryos.

Of course, scaling is more than just a response to spatial constraints. For example, the timing of ecdysone release in the *Drosophila* larvae plays an important role in organ size control (6). The timing of other signals such as insulin (6), prothoracicotropic hormone (73), and Dilp8 (74) are essential in regulating final adult body size. In the early *Drosophila* embryo, an earlier study from our lab has shown that optogenetically perturbing the timing of Bicoid signaling can lead to changes in morphological events, such as cephalic furrow formation (75). In our videos here, we do not see clear differences in the developmental trajectories in the timing of organ formation in embryos of different size. However, there may be more subtle effects that play a role in determining organ size.

Finally, we highlight that organ size can also be influenced by signals from neighboring organs (76,77). Hormonal controls have been well studied in the growth of *Drosophila* organs (6,78), particularly during the larval and pupal stages of development (79–81). The expression pattern of various hormones has also been characterized during embryonic development (82,83). It will be interesting to explore whether the spatial and temporal pattern of hormone action within the embryo is affected by embryo size.

Understanding how organs scale and adapt to size changes remains a major challenge during development. This work suggests that we need new biophysical models to explain how internal organs acquire specific morphologies, particularly when they are not simply growing to a final size.

SUPPORTING MATERIAL

Supporting material can be found online at https://doi.org/10.1016/j.bpj.2021.05.023.

AUTHOR CONTRIBUTIONS

P.T. and T.E.S. designed the study. P.T. performed all experiments and analysis with assistance from H.R. T.E.S. supervised the project and provided advice on statistical and image analysis. P.T. and T.E.S. analyzed the results. P.T. and T.E.S. wrote the manuscript.

REFERENCES

1. Shingleton, A. W. 2010. Allometry: the study of biological scaling. *Nature Education Knowledge.* 3:2.

2. Boyko, A. R., P. Quignon, …, E. A. Ostrander. 2010. A simple genetic architecture underlies morphological variation in dogs. *PLoS Biol.* 8:e1000451.

3. Thompson, D. A. W. 1917. On Growth and Form. Cambridge University Press, Cambridge, UK.

4. Hariharan, I. K. 2016. Size regulation blossoms in Kobe. *Development.* 143:2691–2695.

5. Nijhout, H. F., and L. W. Grunert. 2010. The cellular and physiological mechanism of wing-body scaling in Manduca sexta. *Science.* 330:1693–1695.

6. Nijhout, H. F., and V. Callier. 2015. Developmental mechanisms of body size and wing-body scaling in insects. *Annu. Rev. Entomol.* 60:141–156.

7. Hariharan, I. K. 2015. Organ size control: lessons from Drosophila. *Dev. Cell.* 34:255–265.

8. Emlen, D. J., L. Corley Lavine, and B. Ewen-Campen. 2007. On the origin and evolutionary diversification of beetle horns. *Proc. Natl. Acad. Sci. USA.* 104 (Suppl 1):8661–8668.

9. Nijhout, H. F., L. M. Riddiford, …, V. Callier. 2014. The developmental control of size in insects. *Wiley Interdiscip. Rev. Dev. Biol.* 3:113–134.

10. Abouchar, L., M. D. Petkova, …, T. Gregor. 2014. Fly wing vein patterns have spatial reproducibility of a single cell. *J. R. Soc. Interface.* 11:20140443.

11. Shraiman, B. I. 2005. Mechanical feedback as a possible regulator of tissue growth. *Proc. Natl. Acad. Sci. USA.* 102:3318–3323.

12. Wartlick, O., P. Mumcu, …, M. González-Gaitán. 2011. Dynamics of Dpp signaling and proliferation control. *Science.* 331:1154–1159.

13. Farge, E. 2011. Mechanotransduction in development. *Curr. Top. Dev. Biol.* 95:243–265.

14. LeGoff, L., and T. Lecuit. 2015. Mechanical forces and growth in animal tissues. *Cold Spring Harb. Perspect. Biol.* 8:a019232.

15. Hamant, O., and T. E. Saunders. 2020. Shaping organs: shared structural principles across kingdoms. *Annu. Rev. Cell Dev. Biol.* 36:385–410.

16. Bakopoulos, D., L. F. Beadle, …, T. K. Johnson. 2020. Insulin-like signalling influences the coordination of larval hemocyte number with body size in *Drosophila melanogaster*. *G3 (Bethesda).* 10:2213–2220.

17. Moreno, E., L. Valon, …, R. Levayer. 2019. Competition for space induces cell elimination through compaction-driven ERK downregulation. *Curr. Biol.* 29:23–34.e8.

18. Lauschke, V. M., C. D. Tsiairis, …, A. Aulehla. 2013. Scaling of embryonic patterning based on phase-gradient encoding. *Nature.* 493:101–105.

19. Webb, A. B., and A. C. Oates. 2016. Timing by rhythms: daily clocks and developmental rulers. *Dev. Growth Differ.* 58:43–58.

20. Koyama, T., and C. K. Mirth. 2016. Growth-blocking peptides as nutrition-sensitive signals for insulin secretion and body size regulation. *PLoS Biol.* 14:e1002392.

21. Parker, N. F., and A. W. Shingleton. 2011. The coordination of growth among Drosophila organs in response to localized growth-perturbation. *Dev. Biol.* 357:318–325.

22. Umulis, D. M., and H. G. Othmer. 2013. Mechanisms of scaling in pattern formation. *Development.* 140:4830–4843.

23. Amourda, C., and T. E. Saunders. 2017. Gene expression boundary scaling and organ size regulation in the Drosophila embryo. *Dev. Growth Differ.* 59:21–32.

24. Houchmandzadeh, B., E. Wieschaus, and S. Leibler. 2002. Establishment of developmental precision and proportions in the early Drosophila embryo. *Nature.* 415:798–802.

25. Huang, A., and T. E. Saunders. 2020. A matter of time: formation and interpretation of the Bicoid morphogen gradient. *Curr. Top. Dev. Biol.* 137:79–117.

26. Namba, R., T. M. Pazdera, …, J. S. Minden. 1997. Drosophila embryonic pattern repair: how embryos respond to bicoid dosage alteration. *Development.* 124:1393–1403.

27. Huang, A., J. F. Rupprecht, and T. E. Saunders. 2020. Embryonic geometry underlies phenotypic variation in decanalized conditions. *eLife.* 9:e47380.

28. Moss-Taylor, L., A. Upadhyay, …, M. B. O'Connor. 2019. Body size and tissue-scaling is regulated by motoneuron-derived activinß in *Drosophila melanogaster*. *Genetics.* 213:1447–1464.

29. Hironaka, K. I., K. Fujimoto, and T. Nishimura. 2019. Optimal scaling of critical size for metamorphosis in the genus Drosophila. *iScience.* 20:348–358.

30. Mirth, C. K., and A. W. Shingleton. 2012. Integrating body and organ size in Drosophila: recent advances and outstanding problems. *Front. Endocrinol. (Lausanne).* 3:49.

31. Campos-Ortega, J. A., and V. Hartenstein. 1997. The Embryonic Development of Drosophila melanogaster, Second Edition. Springer, Berlin.

32. Windner, S. E., A. Manhart, …, M. K. Baylies. 2019. Nuclear scaling is coordinated among individual nuclei in multinucleated muscle fibers. *Dev. Cell.* 49:48–62.e3.

33. Hozumi, S., R. Maeda, …, K. Matsuno. 2006. An unconventional myosin in Drosophila reverses the default handedness in visceral organs. *Nature.* 440:798–802.

34. Benito-Sipos, J., M. Baumgardt, and S. Thor. 2013. Development of the Drosophila embryonic ventral nerve cord: from neuroectoderm to unique neurons and glia. *In* Patterning and Cell Type Specification in the Developing CNS and PNS. J. L. R. Rubenstein and P. Rakic, eds. Academic Press, pp. 627–644.

35. Olofsson, B., and D. T. Page. 2005. Condensation of the central nervous system in embryonic Drosophila is inhibited by blocking hemocyte migration or neural activity. *Dev. Biol.* 279:233–243.

36. Vogler, G., and R. Bodmer. 2015. Cellular mechanisms of Drosophila heart morphogenesis. *J. Cardiovasc. Dev. Dis.* 2:2–16.

37. Olson, E. N. 2006. Gene regulatory networks in the evolution and development of the heart. *Science.* 313:1922–1927.

38. Lengyel, J. A., and D. D. Iwaki. 2002. It takes guts: the Drosophila hindgut as a model system for organogenesis. *Dev. Biol.* 243:1–19.

39. Wells, R. E., J. D. Barry, …, M. P. Zeidler. 2013. Control of tissue morphology by Fasciclin III-mediated intercellular adhesion. *Development.* 140:3858–3868.

40. Page, D. T., and B. Olofsson. 2008. Multiple roles for apoptosis facilitating condensation of the Drosophila ventral nerve cord. *Genesis.* 46:61–68.

41. Karkali, K., P. Tiwari, …, E. Martin-Blanco. 2021. Condensation of the Drosophila nerve cord is oscillatory and depends on coordinated mechanical interactions. *bioRxiv* https://doi.org/10.1101/2021.02.24.432750.

42. Horne-Badovinac, S., J. Hill, …, D. Bilder. 2012. A screen for round egg mutants in Drosophila identifies tricornered, furry, and misshapen as regulators of egg chamber elongation. *G3 (Bethesda).* 2:371–378.

43. Barlan, K., M. Cetera, and S. Horne-Badovinac. 2017. Fat2 and Lar define a basally localized planar signaling system controlling collective cell migration. *Dev. Cell.* 40:467–477.e5.

44. Han, Z., P. Yi, …, E. N. Olson. 2006. Hand, an evolutionarily conserved bHLH transcription factor required for Drosophila cardiogenesis and hematopoiesis. *Development.* 133:1175–1182.

45. Dutta, D., J. W. Bloor, …, D. P. Kiehart. 2002. Real-time imaging of morphogenetic movements in Drosophila using Gal4-UAS-driven expression of GFP fused to the actin-binding domain of moesin. *Genesis.* 34:146–151.

46. Inaki, M., R. Hatori, …, H. Honda. 2018. Chiral cell sliding drives left-right asymmetric organ twisting. *eLife.* 7:e32506.

47. Bodmer, R., R. J. Wessells, …, H. Dowse. 2005. Heart development and function. *In* Comprehensive Molecular Insect Science L. I. Gilbert, K. Iatrou, and S. Gill, eds. . Elsevier, pp. 199–250.

48. Rotstein, B., and A. Paululat. 2016. On the morphology of the Drosophila heart. *J. Cardiovasc. Dev. Dis.* 3:15.

49. Zhang, S., C. Amourda, …, T. E. Saunders. 2018. Selective filopodia adhesion ensures robust cell matching in the Drosophila heart. *Dev. Cell.* 46:189–203.e4.

50. Zhang, S., X. Teng, …, T. E. Saunders. 2020. Periodic oscillations of myosin-II mechanically proofread cell-cell connections to ensure robust formation of the cardiac vessel. *Curr. Biol.* 30:3364–3377.e4.

51. Pinto-Teixeira, F., N. Konstantinides, and C. Desplan. 2016. Programmed cell death acts at different stages of Drosophila neurodevelopment to shape the central nervous system. *FEBS Lett.* 590:2435–2453.

52. Iwaki, D. D., K. A. Johansen, …, J. A. Lengyel. 2001. drumstick, bowl, and lines are required for patterning and cell rearrangement in the Drosophila embryonic hindgut. *Dev. Biol.* 240:611–626.

53. Nakamura, M., K. Matsumoto, …, K. Matsuno. 2013. Reduced cell number in the hindgut epithelium disrupts hindgut left-right asymmetry in a mutant of pebble, encoding a RhoGEF, in Drosophila embryos. *Mech. Dev.* 130:169–180.

54. Hamaratoglu, F., A. M. de Lachapelle, …, M. Affolter. 2011. Dpp signaling activity requires Pentagone to scale with tissue size in the growing Drosophila wing imaginal disc. *PLoS Biol.* 9:e1001182.

55. Petkova, M. D., G. Tkačik, …, T. Gregor. 2019. Optimal decoding of cellular identities in a genetic network. *Cell.* 176:844–855.e15.

56. Little, S. C., M. Tikhonov, and T. Gregor. 2013. Precise developmental gene expression arises from globally stochastic transcriptional activity. *Cell.* 154:789–800.

57. Mirth, C. K., and A. W. Shingleton. 2019. Coordinating development: how do animals integrate plastic and robust developmental processes? *Front. Cell Dev. Biol.* 7:8.

58. Mendes, C. C., and C. K. Mirth. 2016. Stage-specific plasticity in ovary size is regulated by insulin/insulin-like growth factor and ecdysone signaling in Drosophila. *Genetics.* 202:703–719.

59. Shingleton, A. W., J. Das, …, D. L. Stern. 2005. The temporal requirements for insulin signaling during development in Drosophila. *PLoS Biol.* 3:e289.

60. Cheng, L. Y., A. P. Bailey, …, A. P. Gould. 2011. Anaplastic lymphoma kinase spares organ growth during nutrient restriction in Drosophila. *Cell.* 146:435–447.

61. Cobham, A. E., B. Neumann, and C. K. Mirth. 2020. Maintaining robust size across environmental conditions is achieved through plastic growth dynamics in the central nervous system of *Drosophila melanogaster*. *bioRxiv* https://doi.org/10.1101/2020.09.01.277046.

62. Karkali, K., T. E. Saunders, …, E. Martín-Blanco. 2020. JNK signaling in pioneer neurons directs the architectural organization of the CNS

and coordinates the motor activity of the Drosophila embryo. *bioRxiv* https://doi.org/10.1101/092486.

63. Valon, L., and R. Levayer. 2019. Dying under pressure: cellular characterisation and in vivo functions of cell death induced by compaction. *Biol. Cell.* 111:51–66.

64. Liang, J., S. Balachandra, …, L. E. O'Brien. 2017. Feedback regulation of steady-state epithelial turnover and organ size. *Nature.* 548:588–591.

65. Lehmacher, C., B. Abeln, and A. Paululat. 2012. The ultrastructure of Drosophila heart cells. *Arthropod Struct. Dev.* 41:459–474.

66. Hudry, B., S. Khadayate, and I. Miguel-Aliaga. 2016. The sexual identity of adult intestinal stem cells controls organ size and plasticity. *Nature.* 530:344–348.

67. Inomata, H., T. Shibata, …, Y. Sasai. 2013. Scaling of dorsal-ventral patterning by embryo size-dependent degradation of Spemann's organizer signals. *Cell.* 153:1296–1311.

68. Gibeaux, R., K. Miller, …, R. Heald. 2018. *Xenopus* hybrids provide insight into cell and organism size control. *Front. Physiol.* 9:1758.

69. Fish, J. L., R. S. Sklar, …, R. A. Schneider. 2014. Multiple developmental mechanisms regulate species-specific jaw size. *Development.* 141:674–684.

70. Orietti, L. C., V. S. Rosa, …, M. Zernicka-Goetz. 2021. Embryo size regulates the timing and mechanism of pluripotent tissue morphogenesis. *Stem Cell Reports.* 16:1182–1196.

71. Moore, K. L., T. V. N. Persaud, and M. G. Torchia. 2016. The Developing Human: Clinically Oriented Embryology. Elsevier, Philadelphia, PA.

72. Aegerter-Wilmsen, T., M. B. Heimlicher, …, K. Basler. 2012. Integrating force-sensing and signaling pathways in a model for the regulation of wing imaginal disc size. *Development.* 139:3221–3231.

73. McBrayer, Z., H. Ono, …, M. B. O'Connor. 2007. Prothoracicotropic hormone regulates developmental timing and body size in Drosophila. *Dev. Cell.* 13:857–871.

74. Colombani, J., D. S. Andersen, and P. Léopold. 2012. Secreted peptide Dilp8 coordinates Drosophila tissue growth with developmental timing. *Science.* 336:582–585.

75. Huang, A., C. Amourda, …, T. E. Saunders. 2017. Decoding temporal interpretation of the morphogen Bicoid in the early *Drosophila* embryo. *eLife.* 6:e26258.

76. Droujinine, I. A., and N. Perrimon. 2016. Interorgan communication pathways in physiology: focus on Drosophila. *Annu. Rev. Genet.* 50:539–570.

77. Song, W., D. Cheng, …, N. Perrimon. 2017. Midgut-derived activin regulates glucagon-like action in the fat body and glycemic control. *Cell Metab.* 25:386–399.

78. Parker, J., and G. Struhl. 2020. Control of *Drosophila* wing size by morphogen range and hormonal gating. *Proc. Natl. Acad. Sci. USA.* 117:31935–31944.

79. Ahmad, M., L. He, and N. Perrimon. 2020. Regulation of insulin and adipokinetic hormone/glucagon production in flies. *Wiley Interdiscip. Rev. Dev. Biol.* 9:e360.

80. Hyun, S. 2018. Body size regulation by maturation steroid hormones: a *Drosophila* perspective. *Front. Zool.* 15:44.

81. Texada, M. J., T. Koyama, and K. Rewitz. 2020. Regulation of body size and growth control. *Genetics.* 216:269–313.

82. Kozlova, T., and C. S. Thummel. 2003. Essential roles for ecdysone signaling during Drosophila mid-embryonic development. *Science.* 301:1911–1914.

83. Sullivan, A. A., and C. S. Thummel. 2003. Temporal profiles of nuclear receptor gene expression reveal coordinate transcriptional responses during Drosophila development. *Mol. Endocrinol.* 17:2125–2137.